28-GHz Foldable Reflectarray

A Senior Honors Project

Presented to the Faculty of the Department of Electrical Engineering,

University of Hawaii at Manoa

In Partial Fulfillment of the Requirements

For Bachelor of Science in Electrical Engineering with Honors

By Deolian Domawa

Fall 2025

Mentor:

Dr. Aaron Ohta

Committee:

Dr. Wayne Shiroma

Acknowledgements

This project would not have been possible without the guidance and encouragement of Dr. Aaron Ohta and Dr. Wayne Shiroma through their expertise in fabrication and RF antennas. Their support throughout the duration of this project and my time with the Liquid Metal Electronics team has allowed me to explore the RF side of engineering and has contributed to my academic growth. I would also like to give my gratitude to my graduate mentors, Saige Dacuycuy and Glan Manio who have assisted me with fabrication and testing, and provided feedback to the project which furthered my understanding of the antennas.

Abstract

The high-speed, low-latency wireless communication in 5G and future 6G networks require antenna systems that are capable of mitigating propagation loss at millimeter-wave frequencies. This project presents the design, simulation, and testing of a foldable 28-GHz reflectarray antenna that can change the directivity of reflected signals. With higher directivity, the reflectarray would be able to reflect signals to specified end-users that are farther away or need a higher signal-to-noise ratio. With lower directivity, signals can be reflected to multiple end-users that are closer to the reflectarray or are able to function with a lower signal-to-noise ratio. A unit cell of the array was designed using simulation tools to provide a 180° phase difference using two different configurations. Multiple instances of the unit cell form the reflectarray. An 8 row by 4 column reflectarray produced asymmetrical beam reflections with wider beamwidths due to the coarse phase gradient and its smaller aperture, signifying lower directivity. Increasing periodicity by expanding the aperture size to an 8x8 strengthened reflected power, and improved directivity by narrowing half-power beamwidth. Experimental results confirmed that enlarging the aperture improved reflected power and directivity. However, physically-folded reflectarrays had a more imprecise beam-steering ability, which can be attributed to capacitive coupling between the two halves of the array. Overall, this study demonstrates that a foldable reflectarray can be expanded to improve directivity and reflected power.

Keywords: Reflectarray, 5G, directivity, antenna

Table of Contents

List of Figures

I. Introduction

With the expansion of 5G networks and ongoing research toward 6G communication systems, advancements on high-frequency wireless connections would allow for faster data transmission with lower latency as the available bandwidth increases [1]. However, a major challenge as frequencies continue to increase is propagation loss and attenuation which limits coverage and signal reliability. More specifically, high-frequency electromagnetic waves experience higher loss as they travel longer distances, and environmental conditions like the weather and molecules in the air can further contribute to the absorption and dissipation of energy. Physical obstacles also become harder for signals to propagate through, leading to substantial losses when encountering buildings, trees, or even human bodies. Due to these effects, millimeter waves (mmWave), electromagnetic (EM) waves with frequencies ranging from 30 to 300 GHz [2] have shorter effective communication ranges and are more susceptible to being blocked or scattered by the environment. These limitations create a need for communication systems that are capable of compensating for high propagation losses.

A common solution to compensate for signal loss is to focus signals efficiently toward a specified direction of which a reflectarray antenna, a surface made of conductive elements, is capable of by controlling the reflected phase of incoming EM waves, similar to a parabolic reflector but more portable. As such, as the operating frequencies of communication systems have continued to increase over the years, advances in antenna design have been explored extensively, and modern evolution of the traditional reflectarray concept has led to the development of reconfigurable intelligent surfaces (RIS), which use electronically tunable components such as PIN

diodes, varactor diodes, or liquid crystal substrates to dynamically modify phase reflections [3]. While RIS designs offer flexibility, power and complex circuitry to control electrical components are required, increasing cost and fabrication difficulty.

To address these challenges, this project explores a 28-GHz foldable reflectarray antenna that is designed to control its directivity by manipulating the aperture size. The final prototype serves as a proof of concept demonstrating that increasing the aperture size by unfolding the reflectarray enhances directivity and reflected power, whereas reducing the aperture size reduces directivity and reflected power.

Significance

Many conventional designs employ other configurations to enhance the efficiency of a reflectarray by achieving a wider bandwidth or dual-polarization which improves the robustness of the reflected signals [4]. Some examples are multi-layered reflectarrays that achieve a wider bandwidth at the expense of being thicker and complex to fabricate, and multi-resonant designs that can operate at multi-frequencies but require complex geometries that have smaller fabrication tolerances [5][6]. More recently, reflectarrays incorporate an RIS design that utilizes elements that can be configured electrically, such as PIN diodes, varactor diodes, or liquid crystal substrates. The Liquid-Metal Electronics VIP team at the University of Hawaii at Manoa, for example, have demonstrated reconfigurable reflectarrays consisting of liquid metal elements actuated by voltage. However, this required a complex and lengthy fabrication process.

Given these challenges, a foldable reflectarray with a simple design is highly desirable. This combines portability and limited reconfigurability, enabling adjustments

in the directivity and reflected power of signals without significant fabrication or design complexity, and eliminating the need for electrical power.

How Reflectarrays Work

Wireless communication signals are made up of electromagnetic (EM) waves characterized by their amplitude, frequency, and phase. When an EM wave strikes a surface as shown in Figure 1, each point on that surface reflects the wave with some phase, which is its position in its cycle where 2π or $360°$ is a full cycle.

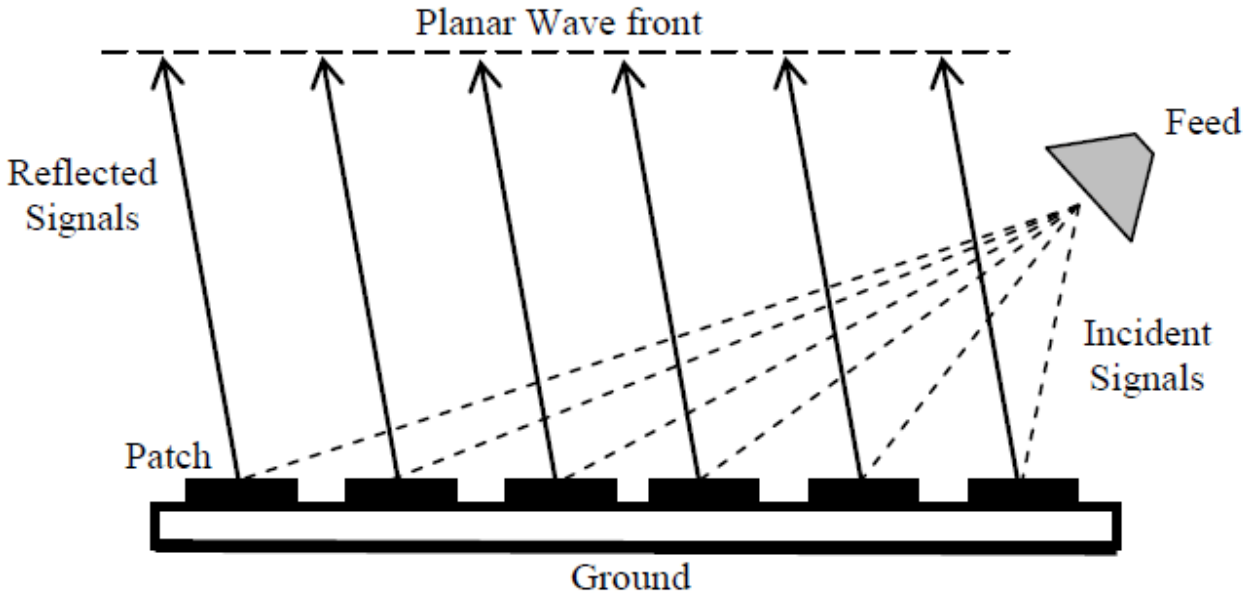

Figure 1. A side-view of a reflectarray with each conductive elements reflecting signals, forming a wavefront. Figure reproduced from [7].

If a surface has the same structure throughout like a simple copper sheet, it is very likely that it would reflect with the same phase. The reflected waves combine in-phase only along the normal direction resulting in a normal reflection, or if it were incident at $45°$ from the surface, it would also reflect at $45°$ from the surface towards the

opposite direction as predicted by the conventional Snell's Law. To focus or steer the reflected beam in a desired direction, there must be a progressive phase shift across the surface. This is how a reflectarray operates. [8]

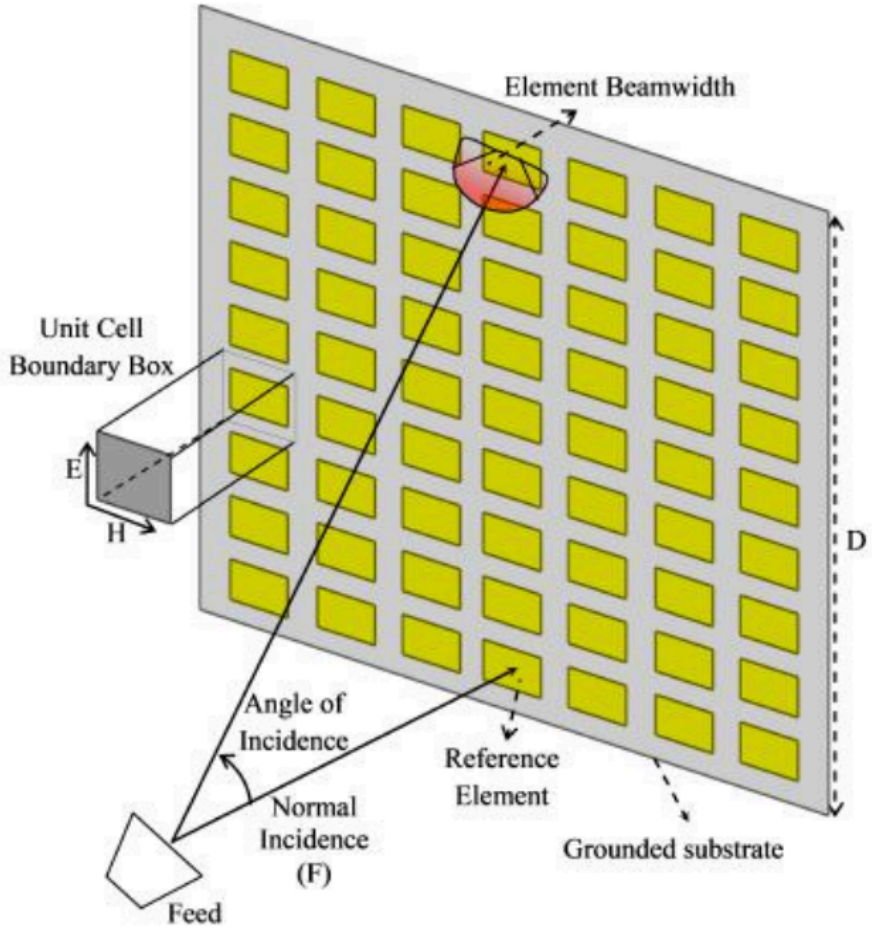

Fig. 2. General structure of a reflectarray with a transmitter horn. Figure reproduced from [9].

A reflectarray consists of a flat surface made up of smaller elements called unit cells, portrayed as the yellow boxes in Figure 2. Each unit cell is capable of reflecting incident electromagnetic waves with a specific phase shift using conductive patches of

varying geometry on the surface. When an EM wave collides on the surface of the reflectarray, a surface current is induced on the conductive patches. This current radiates an EM field, acting like a tiny secondary antenna, and its phase depends on the phase of the surface current at that location. By adjusting the geometry or properties of each element like the size of the patch, the phase shift between the incident and reflected waves can be manipulated. A progressive phase shift across the reflectarray surface, ensures that constructive interference made by the reflected wavefronts are in the desired direction.

Methodology

The methodology includes the design, simulation, fabrication, and testing of a foldable 28-GHz reflectarray antenna. The approach was divided into three main stages: unit cell design, reflectarray design, and fabrication and testing. First, a unit cell was designed and simulated using Ansys HFSS software to determine the reflection phase and magnitude at the frequency of 28 GHz. These results were then used to configure the overall reflectarray phase gradient to establish the highest possible phase state in a column-by-column phase shift. Finally, the fabricated arrays were measured to validate the accuracy of the simulation and assess the impact of aperture size and folding geometry on reflected power and directivity.

II. Unit Cell

Unit Cell Simulation

A unit cell is the fundamental building block of a reflectarray, and its design determines how the surface will react to electromagnetic waves. The design process utilized a high-frequency simulation software called Ansys HFSS, as it accurately predicts the reflected amplitude and phase of the unit cell. The simulated results are essential for optimizing the unit cell for the required phase shift with minimal reflection loss.

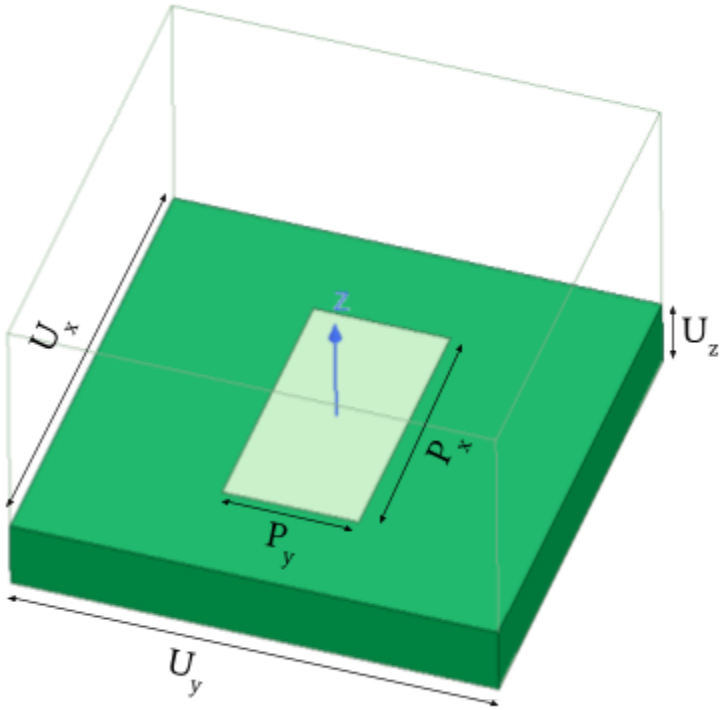

Fig. 3. 28-GHz unit cell model with $U_x = U_y = 5\,mm$, $U_z = 0.7874\,mm$, and $P_y = 1.5\,mm$

The unit cell shown in Figure 3 consists of three components: a rectangular copper patch, a dielectric substrate, and a copper ground plane. To keep the design

simple, the reflectarray has unit cells of a fixed size, and an equal length and width. The dielectric substrate separates the patch from the ground plane, and controls the coupling between these copper elements to reduce losses when reflecting signals. The dielectric substrate was selected for its compatibility with the operating frequency of 28 GHz. The substrate, Rogers Duroid 5880 with a thickness of 31 mil [10], has a dielectric constant of 2.2 and a loss tangent of 0.0009. This low-loss substrate also allows for a manageable unit cell size. For the ground plane, it exists as a conductive backing located below the substrate, and prevents electromagnetic waves from propagating past the substrate by either reflecting or absorbing them. Without the ground plane, part of the incident wave would simply pass through the dielectric without being reflected which decreases the efficiency of the reflectarray.

As the size of the unit cell controls the sample spacing of the reflectarray, too large of a unit cell can result in undersampling where the phase pattern is sampled too coarsely, resulting in energy being re-radiated into unwanted directions. When the unit cell is too small, the patch from adjacent cells can be so close that they interfere with one another. However, some coupling between patches is wanted as it increases the phase range that can be offered as the patch length, P_x, is varied throughout the array [11] . The size of a unit cell is typically a fraction of the corresponding wavelength of the frequency it is designed to operate at. For the unit cell described here, this calculation is:

$$\lambda_0 = \frac{c}{f} = \frac{3\times10^8\ m/s}{28\times10^9\ Hz} = 10.7\ mm$$

At a frequency of 28 GHz, the free-space wavelength is 10.7 mm. Based on the study in [11], a cell sized at a half-wavelength resulted in a higher gain compared to a unit cell sized at $\lambda/3$ or $\lambda/4$ (when operating at 32 GHz). Following this find, sizing the 28-GHz unit cell with dimensions of half a wavelength results in U_x and U_y equal to 5.35 mm. For ease of fabrication, these dimensions were rounded down to 5 mm.

For the size of the patch, only the length would be varied throughout the reflectarray, while the width P_y is held constant at 1.5 mm. By keeping the width P_y fixed, the reflectarray design is kept simple and the patches evenly spaced along the y-direction, at the expense of a more limited phase range. If the patches that make up the phase gradient were also varied in P_y, determining the patch sizes would require a parametric sweep of those two variables instead of only P_x, resulting in a longer sweep that can be time-consuming.

Unit Cell Simulation Results

A parametric sweep of the unit cell was simulated to evaluate the design's efficiency and phase response with different patch lengths. To form the reflectarray, a column-based periodic pattern for arranging the cells was implemented in which all cells in a given row are identical while differing from column to column, thereby producing periodicity along the y-direction [12]. The parametric sweep was performed on P_x from 1.0 mm to 4.0 mm at a step size of 0.1 mm. The frequency sweep was conducted from 25 GHz to 30 GHz.

Analysis of Unit Cell Simulation Results

In Figure 4, it can be seen that all values of P_x resulted in reflection coefficient magnitudes of 0.9910 or greater. The high values of the magnitude of the reflection coefficient means that any patch length will suffice in maintaining a low power loss, as the highest possible loss would be 0.9%. However, in Figure 5 where the reflection phase of different patch lengths are shown, there is a phase range that no value of P_x would be capable of achieving. Figure 6 clearly visualizes this phase gap by the lack of data points between 130° to 170°. To clarify, P_x at its lowest value of 1.0 mm has a reflection phase of +120.5°, and -174.6° at its highest value of 4.0 mm. With a difference of 295.1°, the unit cell would be incapable of completing a complete 360° phase range depending on how many phase states are implemented in the reflectarray as the cell cannot fulfill the remaining 64.9°. For example, increasing the number of phase states to a 3-bit reflectarray would require a phase difference of 45° between adjacent states, which cannot be fulfilled by the current unit cell. The most phase states possible that can accomplish a complete 360° phase range would be with a 2-bit array that has four states as the reflectarray would require the adjacent states to have an approximate 90° phase difference, making the 64.9° that the unit cell is unable to fulfill become irrelevant. However, with the parameters that were swept, a 2-bit array would still be difficult to achieve as the current parameters that had been simulated can roughly maintain a 90° phase difference between adjacent states. The simulation would require a finer parametric sweep to determine the closest P_x values, but the step size would be smaller than 0.1 mm. The number of patch length to sweep would increase significantly, resulting in a longer simulation time. Furthermore, the fabrication tolerance would be

smaller as there would hardly be a difference between fabricating a patch with a length of 3.0 mm versus a 3.01 mm, making it phase-sensitive.

As a result, a 1-bit array was designed as it would only need two states which have a 180° phase difference. The difference was achieved with P_x values of 3 mm and 3.7 mm, which have a phase of 25° and 204.8°, respectively. The difference is 179.8°, a very close approximation of 180°. The downside of a large phase difference is that it made the phase gradient of the reflectarray coarse.

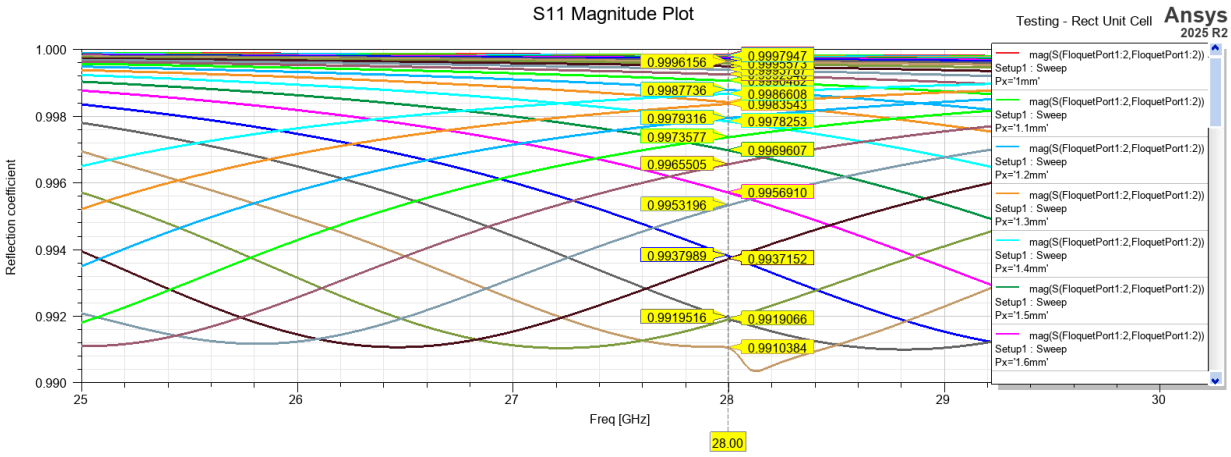

Fig. 4. Plot of reflection coefficient versus frequency with parametric sweep of P_x from 1.0 mm to 4.0 mm at step size of 0.1 mm

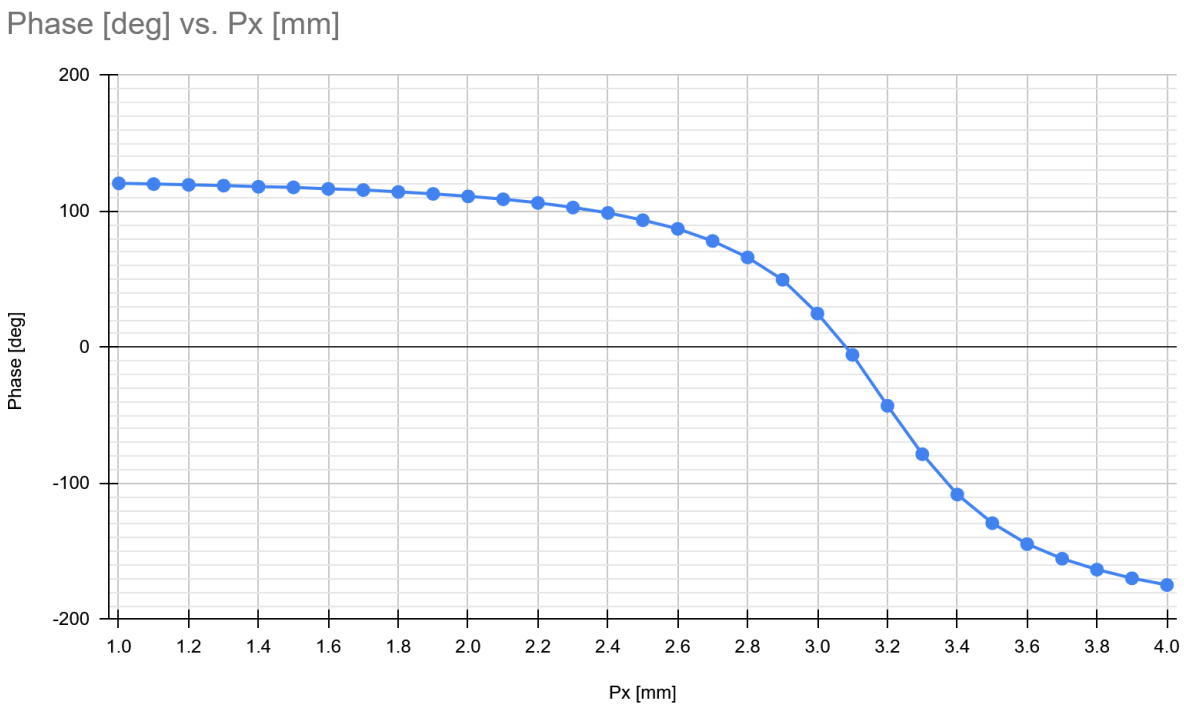

Fig. 5. Plot of reflection phase versus patch length with $P_y = 1.5\ mm$ at 28 GHz

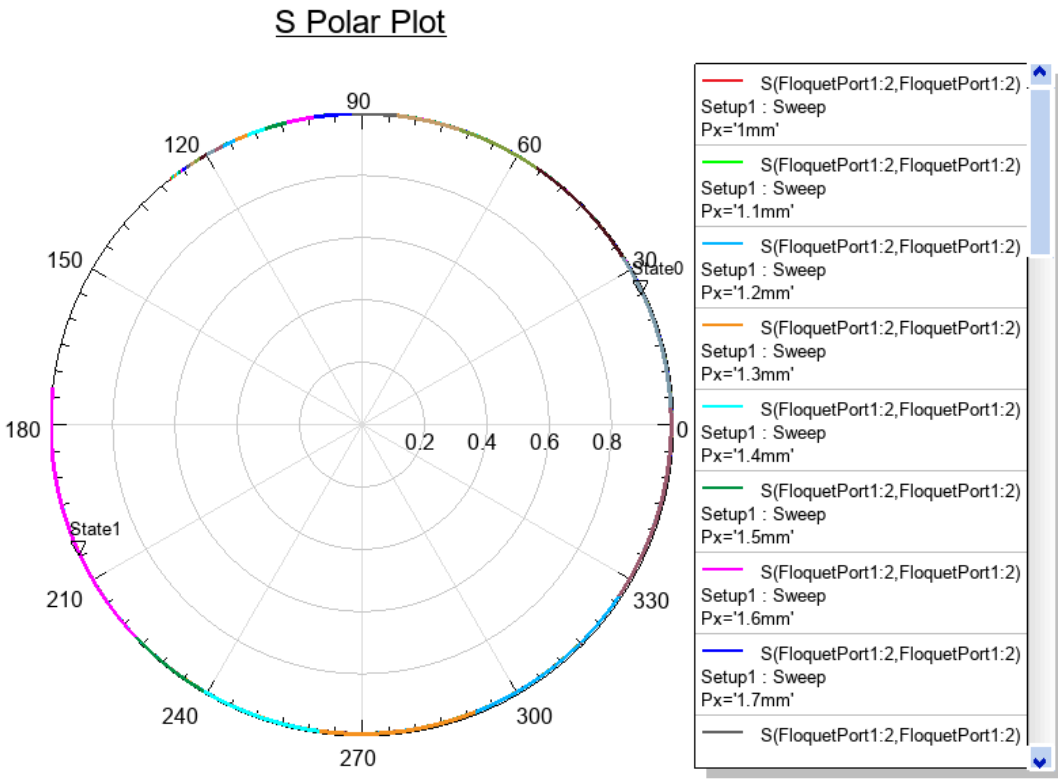

Fig. 6 Polar plot of S parameters with parametric sweep of P_x from 1.0 mm to 4.0 mm at step size of 0.1 mm

III. Reflectarray

Reflectarray Simulation

When the simulation of the unit cell was completed, the reflectarray was designed to be 1-bit with two phase states, State 0 and State 1, which are distributed by column. Following a 0011 pattern, an 8x4 array was simulated as shown in Figure 7a.

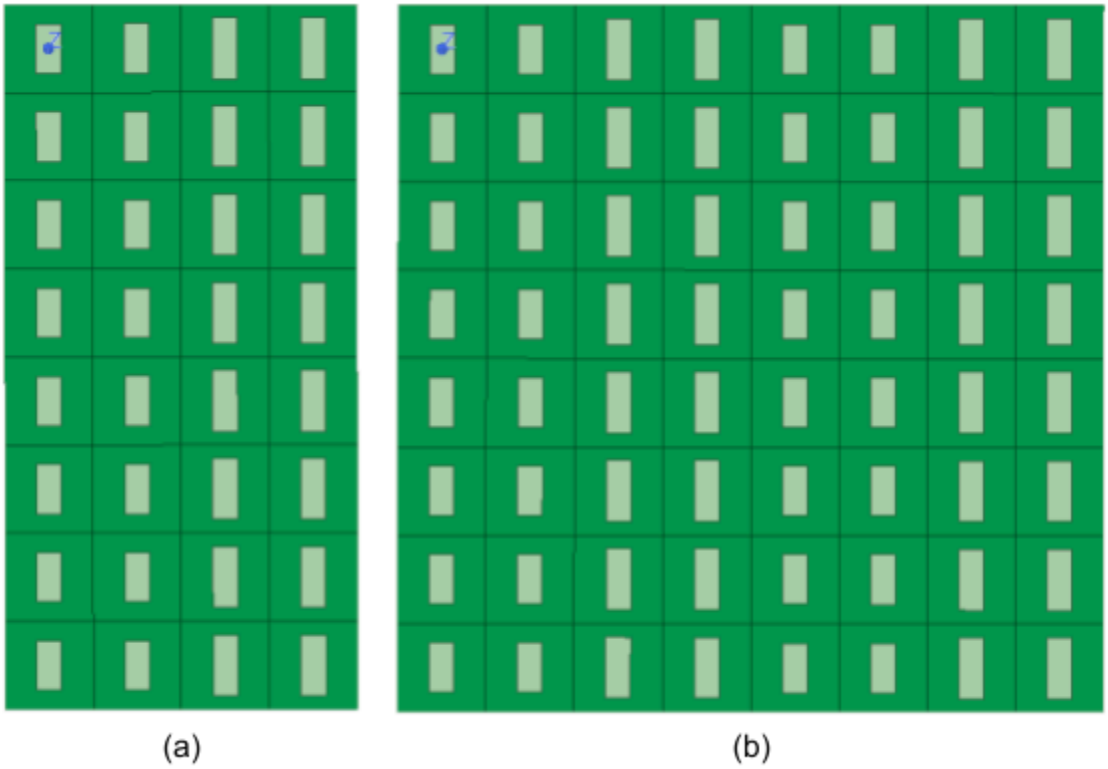

Fig. 7. An (a) 8x4 simulated reflectarray model with P_x for the first two columns on the left being 3.0 mm (State 0), and 3.7 mm (State 1) for the last two; and (b) 8x8 made up by two 8x4 arrays side-by-side

With the phase gradient of the reflectarray, the anomalous reflection can be predicted by the Generalized Snell's Law of Reflection [13].

$$\theta_r = sin^{-1}\left(\frac{\lambda_0}{360°}\frac{d\phi}{dx}\right) = sin^{-1}\left(\frac{0.0107m}{360°}\frac{179.8°}{2\times 0.005m}\right) = 32.3°$$

Based on the calculation above in which $d\phi$ represents the total phase difference between the adjacent states and dx is the periodic spacing before the change in state, the 1-bit array should have a beam reflection at angles ±32.3°. If the reflectarray was a 2-bit, the symmetric beam would be eliminated due to a finer gradient [12].

An 8x8 reflectarray was designed to consist of two 8x4 arrays side-by-side as shown in Figure 7b. By increasing the aperture size by extending the columns instead of rows, more periodicity was introduced into the gradient. Therefore, in addition to boosting the reflected power, the directivity of the reflectarray was improved. The foldable aspect of the reflectarray was that the 8x8 array can be folded to form an 8x4 array. This can be done with a 180-degree fold in which the copper ground plane of both halves of the array are flat against one another as shown in Figure 8a. Alternatively, the 8x8 array can be folded 90 degrees, making the array form an L shape as shown in Figure 8b. The L-shaped array has less coupling between the two halves of the array.

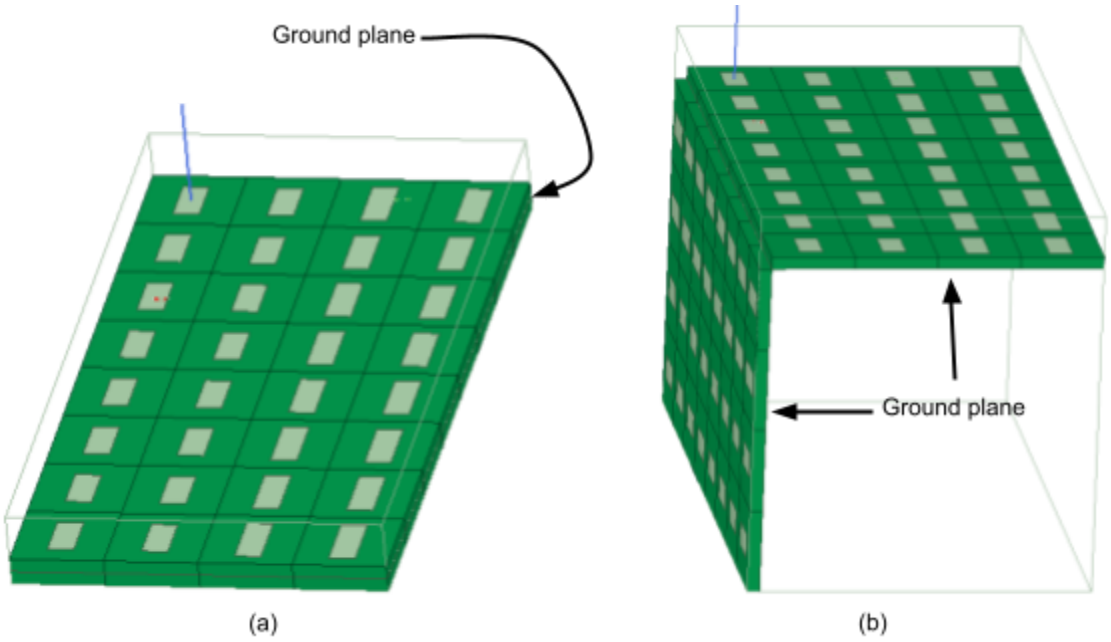

Fig. 8. An 8x8 as a (a) complete fold in which the ground planes are in contact with each other, and (b) partial fold shaped like an L

Reflectarray Simulation Results

The various reflectarray configurations were simulated in Ansys HFSS. Each reflectarray was illuminated with a normally incident plane wave positioned at a distance of $\lambda/4$ from the surface. The simulated results for the unfolded 8 x 8 array (legend: 8x8), a single 8 x 4 array (legend: 8x4), a completely folded array (legend: 8x4 - B2B), and a L-folded array (legend: 8x4 - L) are shown in Figure 9.

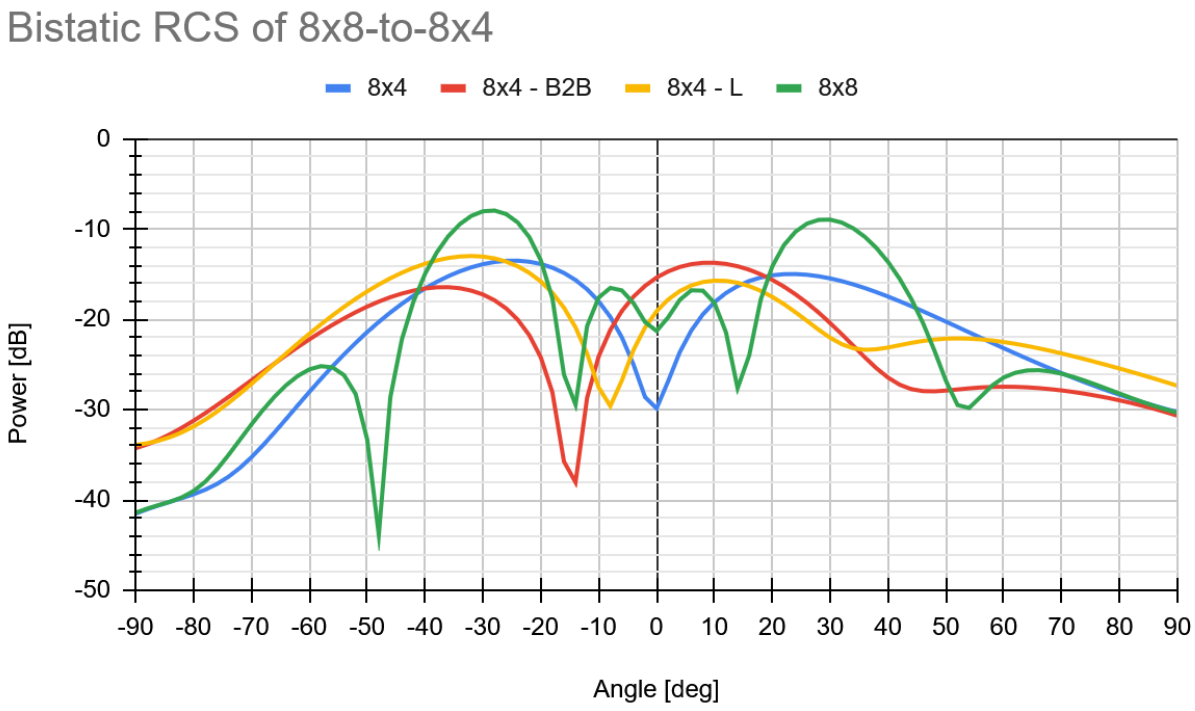

Fig. 9. A bistatic RCS plot in which the arrays in Figure 7a (blue), 7b (green), 8a (red), and 8b (yellow) are simulated

Figure 9 represents the expected bistatic RCS of the reflectarrays by showing the power of signals received at different angles after reflection. The 8x8 (red line) shows an increase in reflected power compared to any of the 8x4 configurations. More specifically, the peak of the major lobes of the 8x8 is -7.95 dB at the reflection angle of -28.05°, and -8.92 dB at 28.19°. The 8x8 reflectarray has at least 6 dB more reflected power compared to any of the 8x4 arrays. This means that the 8x8 array reflects more than four times more power than the 8x4 array configurations. Furthermore, the directivity was shown to have improved when comparing the half-power beam width (HPBW) of the major lobes which represents the angle between the points where the

gain drops by half its peak power (-3 dB). The calculated HPBW for the different reflectarray configurations are shown as follows:

$$HPBW_{8x8^-} = 14.28° \,||\, HPBW_{8x8^+} = 15.99°$$

$$HPBW_{8x4^-} = 27.41° \,||\, HPBW_{8x4^+} = 31.69°$$

$$HPBW_{8x4,L^-} = 27.69° \,||\, HPBW_{8x4,L^+} = 24.7°$$

$$HPBW_{8x4,B2B^-} = 28.83° \,||\, HPBW_{8x4,B2B^+} = 18.55°$$

When compared quantitatively, the HPBW of an 8x8 is narrower than any of the 8x4 folds or single 8x4. The results show that the reflected power is concentrated in that narrow angular region of the HPBW.

Analysis of Reflectarray Simulation Results

When comparing the accuracy of the direction in which the arrays were expected to reflect, there are significant discrepancies in reflection angle. In Figure 9, a single 8x4 (blue line) has peaks occurring at -14.99 dB at 22.77° and -13.45 dB at -24.05°, which are shifted 9.53° and 8.25° to the left compared to the angle of 32.3° calculated from the Generalized Snell's Law, respectively. This was very likely due to the 8x4 array having only a single periodicity whereas the Generalized Snell's Law assumes a continuous or finely sampled phase gradient. With only one period in which the 0011 pattern is present, there are not enough samples. This explains why when unfolded to an 8x8, the reflection angles were -28.05° and 28.19°, which are closer to 32.3°. If the

design was expanded to be an 8x12 reflectarray, it should match even closer to the expected angle.

Another issue presented by the data in Figure 9 is the asymmetry that occurs when the 8x8 is partially or completely folded to an 8x4. Compared to a single 8x4 array, there is an obvious shift to the major lobes. To be more precise, a partial fold (yellow line) results in about a 7.86° to 11.78° shift to the left, and a complete fold (red line) also shifts the peak to the left by about 13.68° to 15.71°, the latter fold showing a larger mismatch. This means that folding does affect the reflection angle, and the reflectarray may not direct signals as accurately as expected.

Overall, the simulation shows that the 8x4 reflectarray configurations will have a broader beamwidth, allowing signals to cover a wider area and reach more end-users spaced farther apart, requiring less precise beam-steering which is ideal due to the shifting that occurs with a folded reflectarray. Additionally, it is more suitable for users located closer to the antenna as it delivers lower reflected power. The 8x8 array exhibited a narrower beamwidth and higher reflected power, which is more ideal for fewer targeted end-users that are farther away from the antenna. However, it would be best to test this observation out on a bigger array that has enough periodicity to assume Generalize Snell's Law, as the lack of samples in an 8x4 could have contributed to the discrepancies.

Reflectarray Fabrication

The reflectarray was then fabricated and tested in an antenna range to compare its performance to the simulation. As previously stated, the substrate that was used was a 5880 Rogers Duroid that had a thickness of 31 mil, and an 18-μm-thick

electrodeposited copper foil on both sides. With the two 8x4 arrays already milled and coated with positive photoresist by one of the graduate mentors, only the etching process remained to be completed. The copper patches were etched using mixtures of DI water and ferric chloride hexahydrate as shown in Figure 10 before cutting away the copper around the array using a guillotine paper cutter.

Fig. 10. Excess copper being etched in DI water and ferric chloride hexahydrate mixture

The 8x4 arrays were measured to be 43 mm x 22 mm instead of 40 mm x 20 mm. It has a diagonal percent error of 8.0%, though the patches were spaced accurately.

IV. Testing

Testing

With the two 8x4 arrays setup as shown in Figure 11 with different reflectarray configurations, the arrays were binded together using a blue painters tape. To keep it held onto the holder, it was taped directly on a ferrite sheet using a small piece of double-sided kapton tape. These configurations were tested inside a MilliBox chamber insulated with anechoic foams and a setup as illustrated in Figure 12.

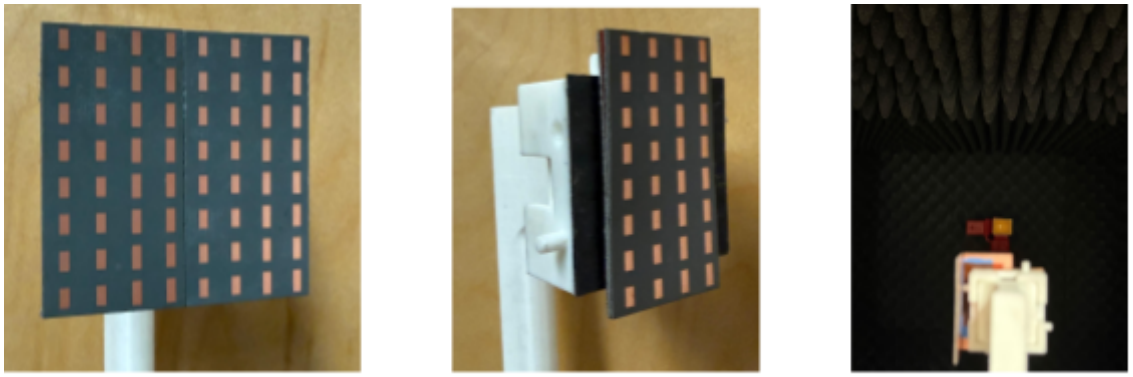

Fig. 11. Setup for (a) an 8x8 array, (b) an 8x4 completely-folded array, and (c) an 8x4 partially-folded array in a MilliBox antenna range with ferrite sheet backing

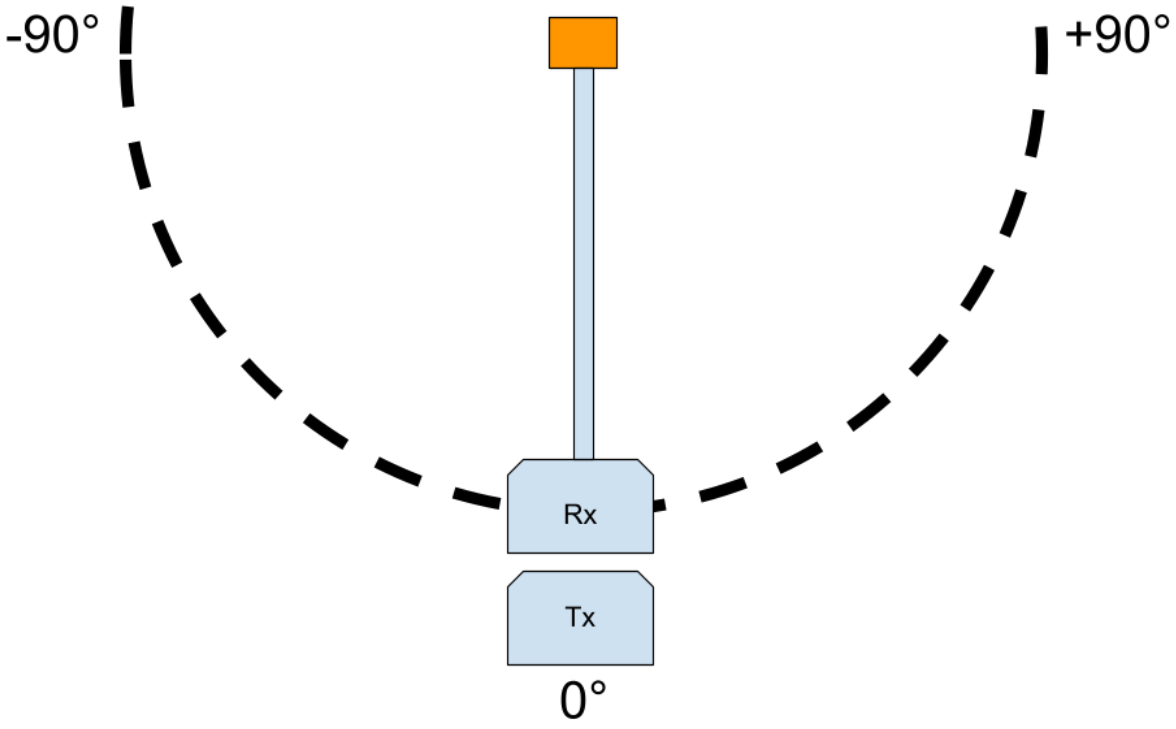

Fig. 12. Antenna range where the orange is the array, Tx is the normal transmit horn antenna, and Rx is the receive horn antenna moving from -90° to +90° in the azimuthal direction

Measured Results

To compare the actual measurements to simulations, all the data were normalized. Before the different folding configurations could be measured, it was important to know how the individual 8x4 arrays performed to ensure that they are performing similarly due to errors that may have been introduced from fabrication. Each graph shows the reflection patterns of the 8x8 and 8x4 array configurations as signals were transmitted at normal incidence. The peaks indicate the angle at which the receiver horn antenna detects the maximum reflected power. In the graph legends, Fabricated L and Fabricated B2B represent the folding configurations in which the 8x8

is completely folded and partially folded to an 8x4, respectively. The Fabricated 8x4 1 and Fabricated 8x4 2 in Figure 13 represents the two 8x4 arrays that were tested individually to ensure matching.

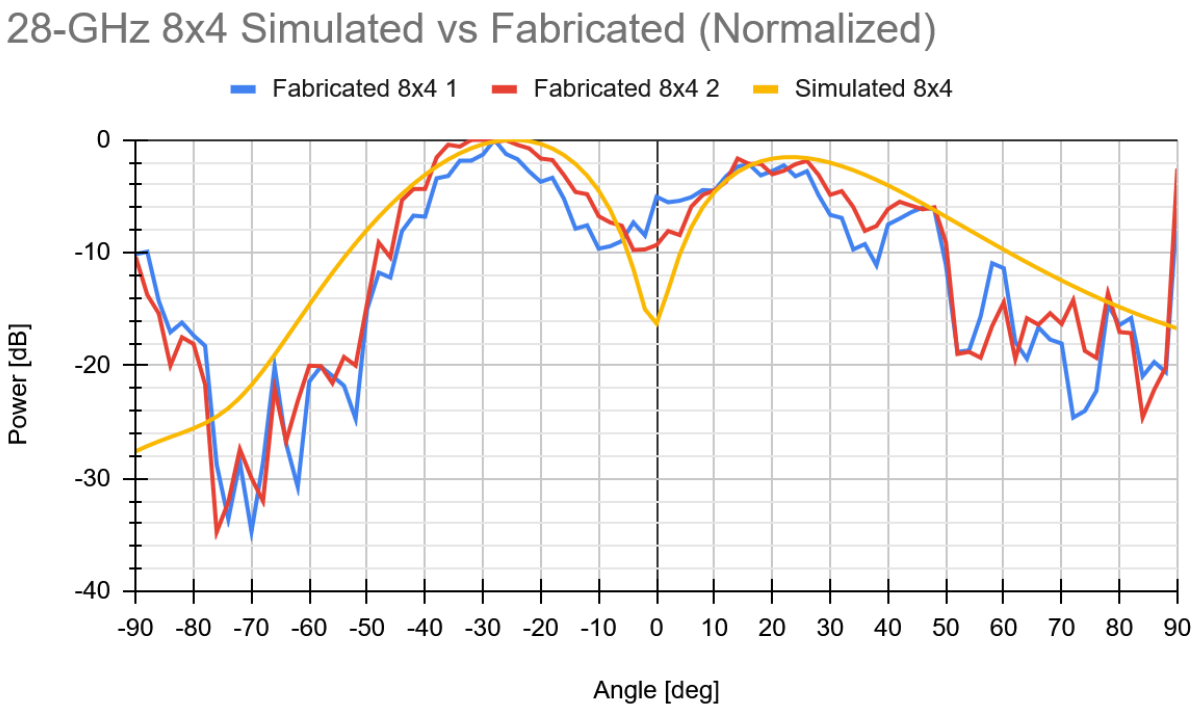

Fig. 13. Normalized plot comparing the two fabricated 8x4 arrays vs the simulation

Based on the results in Figure 13, the fabricated arrays were performing sufficiently similar to the simulated model as the major lobes of the measured results occurred at around +15° and -28°. The trends were relatively consistent as the measurements not only aligned with one another, but also with the simulation.

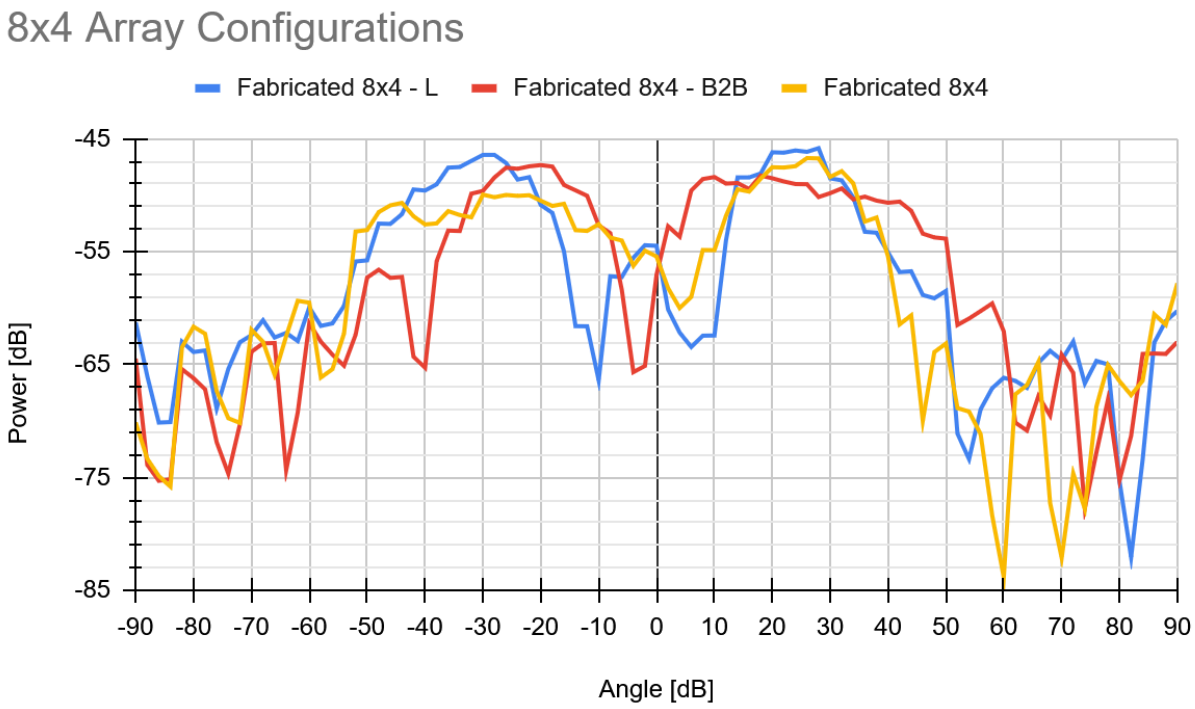

Fig. 14. Measurements for the different 8x4 configurations

Figure 14 shows the un-normalized measurement taken from testing the fabricated 8x4 reflectarrays. After confirming that the two 8x4 arrays performed similarly to one another in Figure 13, since the folding configurations were taken at a different day, the Fabricated 8x4 in Figure 14 is a new measurement taken.

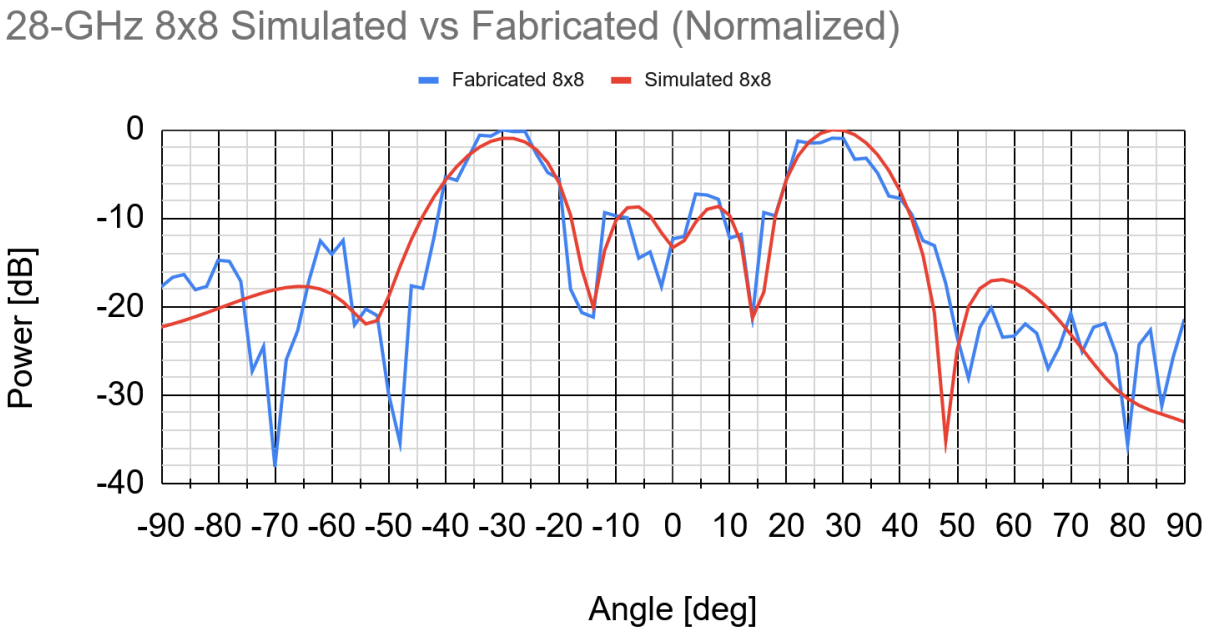

Fig. 15. Normalized plot comparing the actual 8x8 reflectarray and the simulation

Figure 15 gives the normalized data of the fabricated and simulated unfolded reflectarray. While the fabricated 8x8 shows more noise at the tail ends of the graph, it matches very closely to the simulation with two major lobes occurring around ±30° and two minor lobes between the peaks.

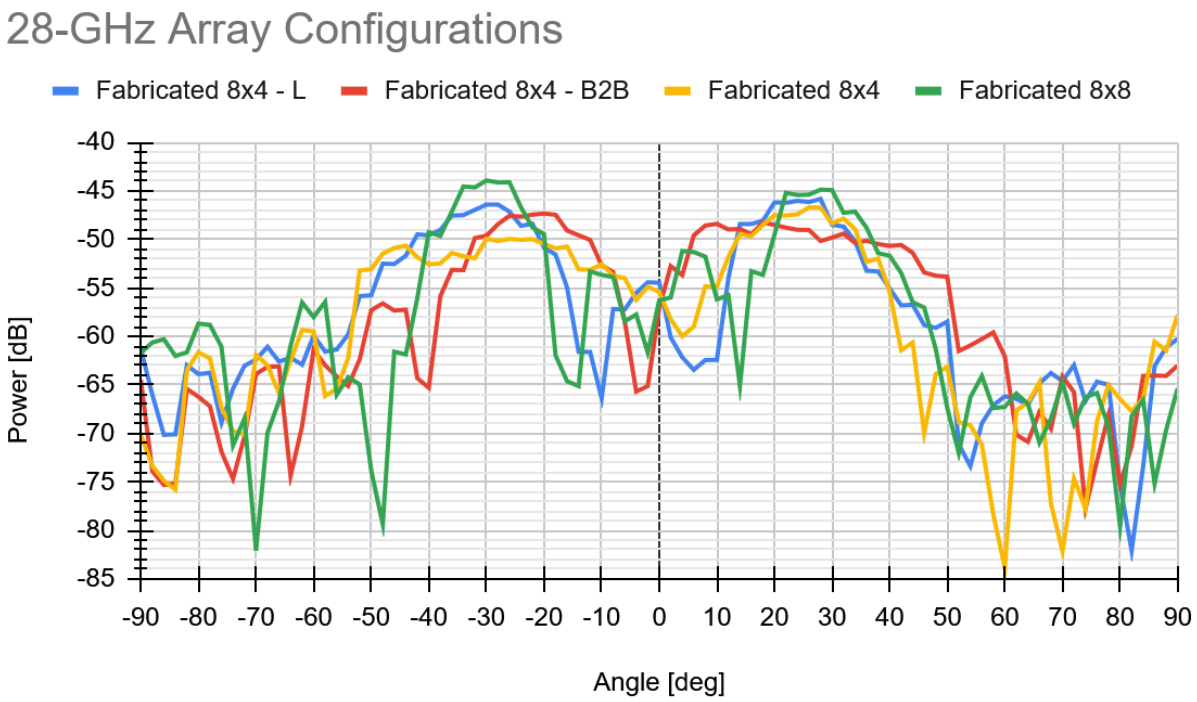

Fig. 16. Measurements of the different 8x4 configurations from Figure 14 overlayed with the fabricated 8x8 data in Figure 15

In this figure, the un-normalized data were graphed to allow for comparison between the different reflectarray configurations on reflected power. The calculated half-power beamwidths are listed below. However, it is important to note that the HPBW calculations are approximate due to noise in real-time testing, which resulted in jagged curves rather than the smoothness portrayed in Figure 9. Additionally, the receiver horn antenna was moved in 2° increments during testing, resulting in missing data between angles, and therefore, the nearest available data values were used in the HPBW estimation.

$$HPBW_{8x8^{-}} = 12^{\circ} \,||\, HPBW_{8x8^{+}} = 16^{\circ}$$

$$HPBW_{8x4^-} = 24° \,||\, HPBW_{8x4^+} = 20°$$

$$HPBW_{8x4,L^-} = 22° \,||\, HPBW_{8x4,L^+} = 22°$$

$$HPBW_{8x4,B2B^-} = 20° \,||\, HPBW_{8x4,B2B^+} = 40°$$

Analysis of Measured Results

When comparing the measurement for the folding configurations in Figure 16, the same observation made from the simulated data could also be seen in the completely-folded reflectarray (B2B). Despite expecting the copper ground plate to supposedly prevent waves from traversing through, it is evident that completely folding the 8x8 to an 8x4 incurs a shift to the reflection angle. When compared to the single fabricated 8x4 (yellow), the B2B configuration (red) appears to have induced a wider beamwidth in the positive reflection angle and a smaller beamwidth in the negative x-axis. The flipped trend between these two configurations on Figure 16 is unexpected as it was ensured that the reflectarrays had the same orientation toward the transmitter horn antenna. This could be due to a distortion occurring heavily on the completely-folded fabricated 8x4 array. However, based on the calculated HPBW, the Fabricated 8x4 - B2B configurations show an 18° increase in beamwidth compared to the Fabricated 8x4 on the positive x-axis, and only a 2° difference on the negative x-axis. Though the completely-folded reflectarray has an unexpectedly wide beamwidth on the positive reflection side, it can be considered advantageous as the antenna has more coverage in exchange of a weaker signal.

The discrepancy between the Fabricated 8x4 and Fabricated 8x4 - B2B may be due to a capacitive coupling that is occurring between the two arrays when their ground plates are directly attached together as the ground plane is not entirely reflecting or absorbing the remaining incident waves that are propagating through the substrate. Running a simulation with a unit cell of this configuration and checking if the phase had shifted compared to the original unit cell could provide some insight into whether it is due to coupling. Otherwise, there is also the possible factor where the ferrite sheet is further distorting reflected signals as it is exposed to the feed horn..

On the other hand, the L configuration in Figure 16, which is the partially-folded reflectarray (blue) reflects 3.52 dB more at -30°. That is more than twice the power of a single 8x4 array. Compared to the simulation, it has a narrower HPBW, though it is only by approximately 2 to 5 degrees which is miniscule due to the rough calculation involved. For the B2B configuration, comparing its HPBW to the simulation, it has a wider beamwidth on the positive x-axis by 21.45° and a smaller beamwidth on the negative x-axis by 8.83°. The capacitive coupling between the two arrays that formed the B2B configuration and the lack of periodicity may have produced a stronger effect in real testing compared to the simulation. Furthermore, the rough estimation in the real HPBW may have also amplified the difference.

Compared to the rest of the configurations, the 8x8 reflectarray performed the closest to its simulation counterpart with only 0.1 to 2.28 degree difference in HPBW. The Fabricated 8x8 demonstrated the highest peak reflected power that is 2.49 dB more than the L configuration at -30° and the smallest HPBW of about 12°, indicating the highest directivity and most focused beam.

V. Conclusion

The development of a foldable reflectarray presented in this project addresses the growing need for portable, high-performing antenna systems as wireless networks move further into the mmWave bands to reduce propagation losses. The design demonstrated that the increase in aperture size through the introduction of more periodicity results in achieving high reflected power and concentrated directivity. Through simulation and real-world measurement, the foldable reflectarray was shown to produce directed reflections consistent with the Generalized Snell's Law when sufficient periodicity was present. The unfolded 8x8 configuration achieved the highest reflected power and the narrowest half-power beamwidth, indicating improved beam focusing and greater directivity. This confirms that increasing the aperture size enhances gain and concentrates the reflected energy into a smaller angular region to compensate for the propagation losses inherent with high frequencies such as 28 GHz.

Discrepancies between the predicted and measured reflection angles for the 8x4 configurations were primarily due to its limited periodicity, which resulted in coarse phase sampling. When expanded to an 8x8 array, the reflected beam aligned more closely with the Generalized Snell's Law output of ±32.3°. The B2B configuration introduced a left shift in reflection angle and an unexpected wide beamwidth , which may have been caused by coupling. This conveys that using the completely-folded reflectarrray may result in a less predictable reflection behavior. As such, further refinement in the folding mechanism may need to be explored. Overall, the results support the motivation behind this project, which is to improve directivity and reflected power by increasing the effective aperture through the unfolding of the reflectarray.

VI. References

[1] “Recent Advances in Extremely-High-Frequency Wireless Networks | IEEE Communications Society,” Comsoc.org, Nov. 15, 2025. https://www.comsoc.org/publications/journals/ieee-tnse/cfp/recent-advances-extremely-high-frequency-wireless-networks (accessed Nov. 07, 2025).

[2] “Millimeter Wave 70/80/90 GHz Service | Federal Communications Commission,” www.fcc.gov. https://www.fcc.gov/wireless/bureau-divisions/broadband-division/microwave-services/millimeter-wave-708090-ghz-service-0

[3] M. I. Abbasi, M. Y. Ismail, Muhammad Ramlee Kamarudin, and Q. H. Abbasi, “Reconfigurable Reflectarray Antenna: A Comparison between Design Using PIN Diodes and Liquid Crystals,” Wireless Communications and Mobile Computing, vol. 2021, no. 1, Jan. 2021, doi: https://doi.org/10.1155/2021/2835638.

[4] J. Tayebpour and R. R. Mansour, "A Wideband Dual-Polarized Reconfigurable Reflectarray Using Polarization Rotation Technique," in IEEE Access, vol. 13, pp. 106906-106915, 2025, doi: 10.1109/ACCESS.2025.3581161.

[5] C. Han, C. Rodenbeck, J. Huang and Kai Chang, "A C/ka dual frequency dual Layer circularly polarized reflectarray antenna with microstrip ring elements," in IEEE Transactions on Antennas and Propagation, vol. 52, no. 11, pp. 2871-2876, Nov. 2004, doi: 10.1109/TAP.2004.835144.

[6] S. -W. Qu, Q. -Y. Chen, J. Li, Q. Chen and M. -Y. Xia, "Single-layer dual-band reflectarray with single linear polarization," 2012 International Conference on Microwave and Millimeter Wave Technology (ICMMT), Shenzhen, China, 2012, pp. 1-3, doi: 10.1109/ICMMT.2012.6230353.

[7] Dahri, Muhammad & Kamarudin, M.R. & Jamaluddin, Mohd haizal & Selvaraju, Raghuraman & Abbasi, Muhammad Inam. (2017). Broadband Resonant Elements for 5G Reflectarray Antenna Design. TELKOMNIKA. 15. 10.12928/TELKOMNIKA.v15i2.6122.

[8] S. A. M. Soliman, E. M. Eldesouki, and A. M. Attiya, “Analysis and Design of an X-Band Reflectarray Antenna for Remote Sensing Satellite System,” Sensors, vol. 22, no. 3, p. 1166, Feb. 2022, doi: https://doi.org/10.3390/s22031166.

[9] M. H. Dahri, M. H. Jamaluddin, M. I. Abbasi, and M. R. Kamarudin, “A Review of Wideband Reflectarray Antennas for 5G Communication Systems,” IEEE Access, vol. 5, pp. 17803–17815, 2017, doi: https://doi.org/10.1109/access.2017.2747844.

[10] Rogers Corporation, , “RT/duroid® 5870/5880 Data Sheet,” Publication no. 92-101 [Revised 08/08/22]. [Online]. Available: https://www.rogerscorp.com/advanced-electronics-solutions/rt-duroid-laminates/rt-duroid-5880-laminates (Accessed Oct. 23, 2025)

[11] Payam Nayeri, F. Yang, and A. Z. Elsherbeni, “BANDWIDTH IMPROVEMENT OF REFLECTARRAY ANTENNAS USING CLOSELY SPACED ELEMENTS,” Progress In Electromagnetics Research C, vol. 18, pp. 19–29, Jan. 2011, doi: https://doi.org/10.2528/pierc10091505.

[12] G. A. Manio, M. T. Kouchi, S. J. Dacuycuy, A. T. Ohta, and W. A. Shiroma, “Rapid Prototyping of Anomalous Reflective Metasurfaces Using Spray-Coated Liquid Metal,” Materials, vol. 17, no. 9, pp. 2003–2003, Apr. 2024, doi: https://doi.org/10.3390/ma17092003.

[13] N. Yu et al., “Light Propagation with Phase Discontinuities: Generalized Laws of Reflection and Refraction,” Science, vol. 334, no. 6054, pp. 333–337, Sep. 2011, doi: https://doi.org/10.1126/science.1210713.